Preprints.org

Article

Not peer-reviewed version

Microstructural Analysis of Sintered Ti–Al–C Composite Powder Materials

Rasa Kandrotaitė Janutienė *, Darius Mažeika, Laura Gegeckienė, Ingrida Venytė, Olha Syzonenko, Andrii Torpakov

Posted Date: 29 November 2023

doi: 10.20944/preprints202311.1870.v1

Keywords: Electron microscopy; Composites; Powder methods; Spark plasma sintering; High voltage electrical discharge; Fullerenes; Intermetallic phase; Graphene

Preprints.org is a free multidiscipline platform providing preprint service that is dedicated to making early versions of research outputs permanently available and citable. Preprints posted at Preprints.org appear in Web of Science, Crossref, Google Scholar, Scilit, Europe PMC.

Copyright: This is an open access article distributed under the Creative Commons Attribution License which permits unrestricted use, distribution, and reproduction in any medium, provided the original work is properly cited.

Preprints (www.preprints.org) | NOT PEER-REVIEWED | Posted: 29 November 2023 doi:10.20944/preprints202311.1870.v1

Disclaimer/Publisher's Note: The statements, opinions, and data contained in all publications are solely those of the individual author(s) and contributor(s) and not of MDPI and/or the editor(s). MDPI and/or the editor(s) disclaim responsibility for any injury to people or property resulting from any ideas, methods, instructions, or products referred to in the content.

Article

Research of Microstructure and Phase Composition of Sintered Ti–Al–C Composites

Rasa Kandrotaitė Janutienė [1,*], Olha Syzonenko [2], Darius Mažeika [1], Laura Gegeckienė [1], Ingrida Venytė [1] and Andrii Torpakov [2]

[1] Kaunas University of Technology, Lithuania; raskand@ktu.lt
[2] Institute of Pulse Processes and Technologies, National Academy of Science of Ukraine; olgasizonenko43@gmail.com
* Correspondence: raskand@ktu.lt; Tel.: +37068696288, Rasa Kandrotaitė Janutienė

Abstract: Titanium-based composite materials arouse interest in such fields like aerospace, transportation, medicine, and other application. Our research project presents the analysis of phase composition of sintered Ti-Al-C composite materials under high voltage electrical discharge. The new technology, described in the previous work allow to synthesize the composites containing various intermetallics, carbides, and nanostructures, as well. The samples of Ti-Al-C powder composites were tested by SEM, Raman spectroscopy and XRD. It was determined that the treatment of the powder by high voltage electrical discharge (HVED) and further sintering at high temperatures using the method of spark plasma sintering (SPS) encourages the formation of the intermetallic reinforcing phases, carbides and different nanocarbon structures like graphene and fullerenes, as well as pure graphite. Intermetallic phases and nanocarbon structures improve mechanical and physical properties of the composites. By using experimental methods mentioned above, the phase composition of Ti-Al-C powder composites obtained at different sintering temperatures was determined. This project is a pilot experimental work, therefore, not all peaks of Raman and XRD were detected, they will be analysed in furture works.

Keywords: SEM; composites; SPS; high voltage electrical discharge; fullerenes; intermetallic phase; graphene; titanium

1. Introduction

Titanium and its alloys are rapidly becoming an important research object in various fields such as the automotive and aerospace industries. These materials are lightweight and have excellent properties such as high specific strength, chemical resistance and biocompatibility. The combination of these attractive properties makes the alloys suitable for structural, chemical, heat resistance, tribological, and biomedical applications [1,2].

Titanium matrix composites (TMCs) are promising metallic materials widely used in various industrial fields, such as medicine, automotive and aircraft industries. TMC materials are characterized by exceptional properties, including relatively low density, as well as high levels of specific strength and corrosion resistance [3].

The high modulus of elasticity of titanium matrix composites is the main indicator of their use in airframes, and the high relative strength has been the impetus for their use in the engine industry. For example, titanium aluminide-based TMCs at 760°C are 50% lighter compared to nickel-based superalloys for high-temperature compressors [4,5].

Titanium-based alloys and composites often contain aluminium due to their excellent properties such as low density, high elastic modulus, high mechanical strength, and high fatigue resistance, which make them widely used in the aerospace, automotive, and transportation sectors [6–8].

Carbon, as a component of titanium alloys and composites, is an excellent heat-resistant material. For example, when used at temperatures above 1000°C, operation from 10 to several 1000

© 2023 by the author(s). Distributed under a Creative Commons CC BY license.

Preprints (www.preprints.org) | NOT PEER-REVIEWED | Posted: 29 November 2023 doi:10.20944/preprints202311.1870.v1

hours is possible, and sometimes approaches 2200°C [9]. The presence of carbon in titanium alloys and composites increases the heat resistance of these materials, increases strength and improves tribological properties.

In Ti-Al-C composites, various processing processes can lead to the formation of the MAX phase, which is a three-layer metal-ceramic material with excellent metal-ceramic properties such as high strength, high hardness, self-lubrication, good electrical and thermal conductivity [10–12]. Ti_3AlC_2 is a typical candidate of the MAX phase and has a multi-layered morphology [13].

Titanium aluminides, such as $AlTi_3$, Al_3Ti or TiAl can be found in Ti-Al-C composite materials. It was determined that during heating in molten salts, the synthesis the MAX phase compounds Ti_2AlC, Ti_3AlC_2, and Ti_2AlC proceeded between 900–1000°C with the formation of auxiliary phases TiC and TiAl, which decreased in abundance with rising the synthesis temperature [14]. After growing of the synthesis temperature to 1300°C, Ti_3AlC_2 appeared together with the phases Ti_2AlC and TiC. It was established that the synthesis of Ti_2AlC allows the formation of initial TiC_{1-x} on graphite and titanium aluminides [14].

The researchers studied the effect of Ti_3AlC_2 content on the physical, mechanical and arc ablation resistance properties of the produced Cu-Ti_3AlC_2 composite, and found that Cu-Ti_3AlC_2 composite properties such as relative density, electrical conductivity, tensile strength and Brinell hardness vary depending on the Ti_3AlC_2 content in the composites. Samples containing 10, 15, 20, 25, 30 and 35 % of Ti_3AlC_2 sintered at 800°C were tested. Since the Ti_3AlC_2 phase has intermediate metallic and ceramic properties, increasing its content in the composite increases the mechanical properties and then starts to decrease [15,16].

In another paper [17], researchers analysed the synthesis, deformation and tribological properties of a new Ti_3AlC_2 – Ti_2AlC MAX phase metal-ceramic composite. The two-phase composition of MAX was synthesized by SPS in a vacuum environment using Ti, Al, and C primary powders. A layered composite was formed, whose deformation mechanism and tribological properties were studied by SEM, TEM, Raman spectroscopy. A detailed analysis of the worn surface showed that the Ti_3AlC_2 - Ti_2AlC two-phase MAX composite is self-lubricating.

After reviewing the literature sources, we can see that Ti-Al-C and other similar systems are widely used in various fields and are constantly researched by scientists from various countries. These materials have excellent physical and mechanical characteristics. The materials we study are characterized not only by the fact that they contain MAX phases and titanium aluminides (intermetallic compounds) in their structure, but also thanks to exposure to a high-voltage electric discharge in kerosene, carbon nanostructures such as graphene, fullerenes, and etc., which is less studied. Therefore, the novelty lies on the specific development of technology of powder treatment allowing to obtain the new composites with improved physical and mechanical properties.

This study helps us to determine the phase composition and microstructure of Ti-Al-C composite powder materials produced by SPS consolidation of the charge after the HVED processing of titanium and aluminium powders in kerosene.

2. Materials and Methods

The samples were prepared from the powder with such composition: 70-75% of titanium and 15% of aluminium. The prepared powder was processed with HVED in liquid kerosene (method is described in detail in [18]). The mass relation of 100 g of hard phase and 1.5 l of kerosene was set to be 1:12. The parameters of HVED are as mentioned here: the stored energy E_1 = 1 kJ and the integral (total) energy E_{sum} = 25 MJ kg^{-1} that is released during the processing of the disperse system. The processing schema is presented in Figure 1.

Preprints (www.preprints.org) | NOT PEER-REVIEWED | Posted: 29 November 2023 doi:10.20944/preprints202311.1870.v1

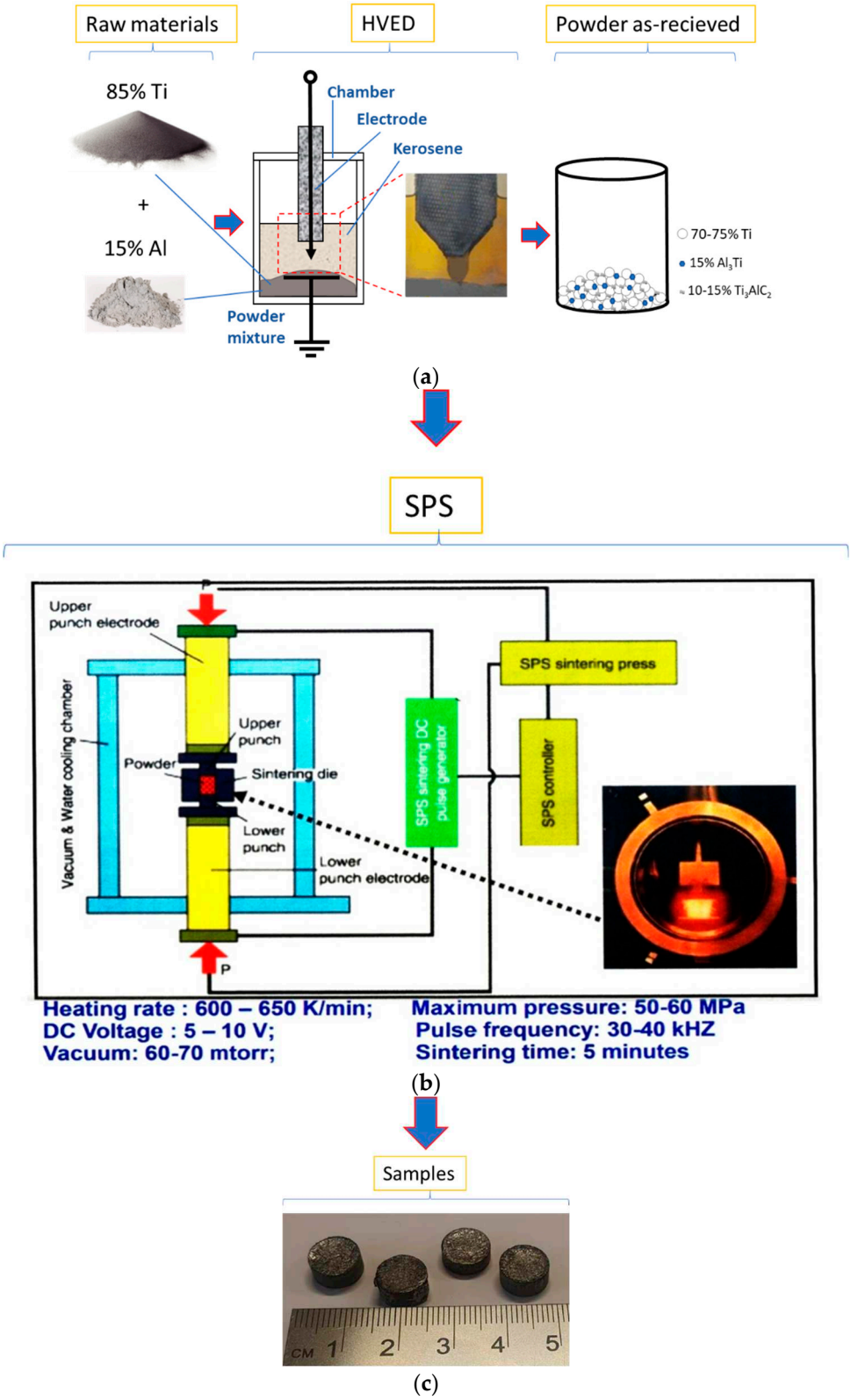

Figure 1. Schema of the preparation of the Ti-Al-C composite powder samples: a) powder treatment by HVED; b) sintering of the samples after HVED; c) samples as received.

The samples were sintered in vacuum under the pressure of 50-60 MPa in a graphitic die between the graphitic electrodes (Figure 1b). The sintering duration was 5 minutes for all samples. The temperature and the current used are presented in Table 1. The samples were designated according to the temperature of sintering and the powder composition after HVED. The experimental plan was made, and the research was performed according to it.

Preprints (www.preprints.org) | NOT PEER-REVIEWED | Posted: 29 November 2023 doi:10.20944/preprints202311.1870.v1

After sintering of the powder, the samples (Figure 1c) were mounted on plastic, ground, and polished with the different suspensions containing 1µ, 0.25µ, and 0.05µ abrasive particles (supplied by Advanced Abrasives Corporation) followed by proper washing. They were explored using ZEISS EVO MA10 scanning electron microscope equipped with the Bruker XFlash 6/10 EDX detector.

The dimensions of cylindrical sintered samples were obtained as Ø8 mm × 5 mm.

Table 1. Data SPS of the powder samples under HVED.

Designation of specimens	Parameters of SPS			Composition of the powder after HVED treatment
	T, °C	I, A	t, min	
G13	950	840	5	75% Ti, 15% Al_3Ti, 10% Ti_3AlC_2
G14	960	770	5	70% Ti, 15% Al_3Ti, 15% Ti_3AlC_2
13	985	995	5	75% Ti, 15% Al_3Ti, 10% Ti_3AlC_2
14	1020	915	5	70% Ti, 15% Al_3Ti, 15% Ti_3AlC_2

An inVia Raman microscope (Renishaw) was used for Raman scattering measurements. The excitation beam was focused on the sample using a 50× objective. Silicon was used for the calibration of Raman setup. Here the parameters of laser:

- 532 nm wavelength.
- Laser power at the sample surface - 3.5 mW.
- Integration time - 10 s.
- Signal was accumulated 10 times.

The Raman Stokes signal was dispersed with a diffraction grating (2400 grooves/mm) and data was recorded using a Peltier cooled charge-coupled device (CCD) detector (1024×256 pixels). This system yields a spectral resolution of about 1 cm^{-1}.

The XRD analysis was carried out on the D8 Advance diffractometer (Bruker AXS, Karlsruhe, Germany). Here are the parameters of the XRD setup:

- The tube voltage of 40 kV.
- The tube current of 40 mA.
- The X-ray beam was filtered with Ni 0.02 mm filter to select the CuKα wavelength (λ = 1.5406 Å).
- Diffraction patterns were recorded using a fast-counting detector Bruker LynxEye based on silicon strip technology.
- Scanning over the range 2θ = 20–90° at a scanning speed of 6°/min using a coupled two theta/theta scan type.

The XRD data of the samples were analysed, and the quantitative determination of the phases was carried out with the Bruker AXS TOPAS 4.1 [19,20] software program using the Rietveld crystal structure refinement method.

3. Results and Discussion

The SEM analysis of the sintered Ti-Al-C powder composites showed that all the samples consisted of a metal matrix and reinforcing particles like carbides and MAX-phases (Figure 2a–c).

It is visible from the micrographs (Figure 2), that the Ti-Al-C powder composites with a heterogenous microstructure contain a huge number of reinforcing particles in the shape of spheres, plates, and needles. The lowest sintering temperature (950°C) gave the biggest number of micro-pores (Figure 2a). With the increased temperature to 960°C and more, the composite became denser with a much lower number of micro-pores (Figure 2b–d).

Preprints (www.preprints.org) | NOT PEER-REVIEWED | Posted: 29 November 2023 doi:10.20944/preprints202311.1870.v1

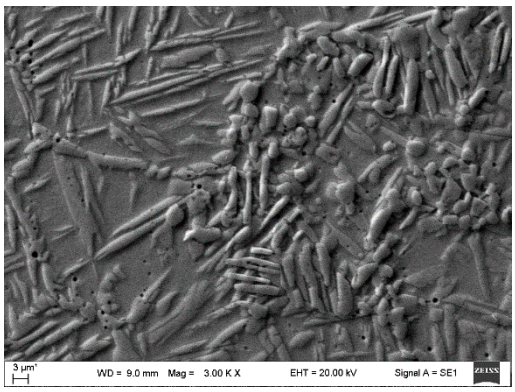

(**a**)

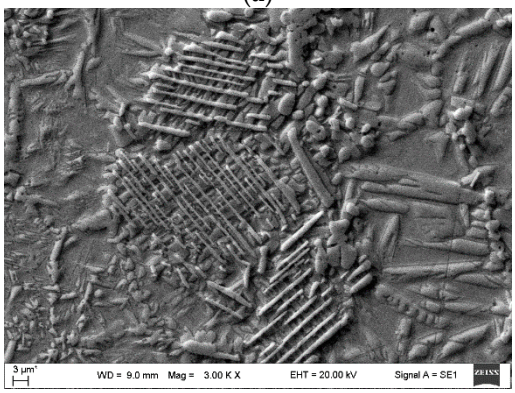

(**b**)

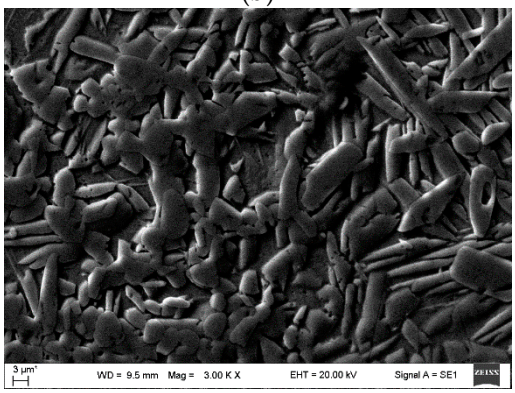

(**c**)

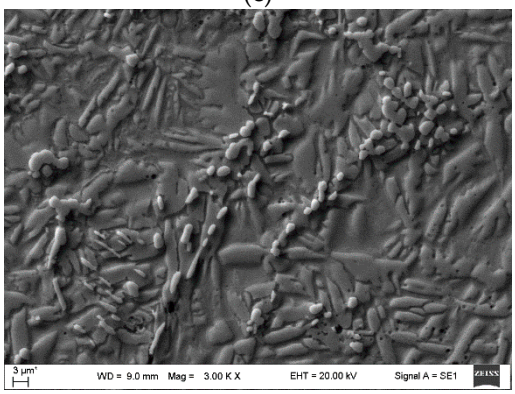

(**d**)

Figure 2. Metal matrix and reinforcing particles (carbides, and intermetallic phases) by SEM analysis: a) sample G13, sintered at 950°C; b) sample G14, sintered at 960°C; c) 13, sintered at 985°C; d) sample 14, sintered at 1020°C.

The X-Ray analysis results from the previous research work showed that strengthening particles were TiC, Ti_3Al and Al_4C_3 when the composition of the as received powder was 80% Ti, 15% Al_3Ti

Preprints (www.preprints.org) | NOT PEER-REVIEWED | Posted: 29 November 2023 doi:10.20944/preprints202311.1870.v1

and 5% Ti_3AlC_2 [18]. For this research we did the elemental mapping of the microstructures with different compositions and sintered at different temperatures of SPS to reveal the distribution of every element in the microstructure and to get data about possible existing reinforcing particles. The mapping micrographs show that the needle-like structure contains more aluminium, and the spherical particles are rich with titanium and carbon (Figure 3). Therefore, we can conclude that the main reinforcing particles can be the carbides of titanium.

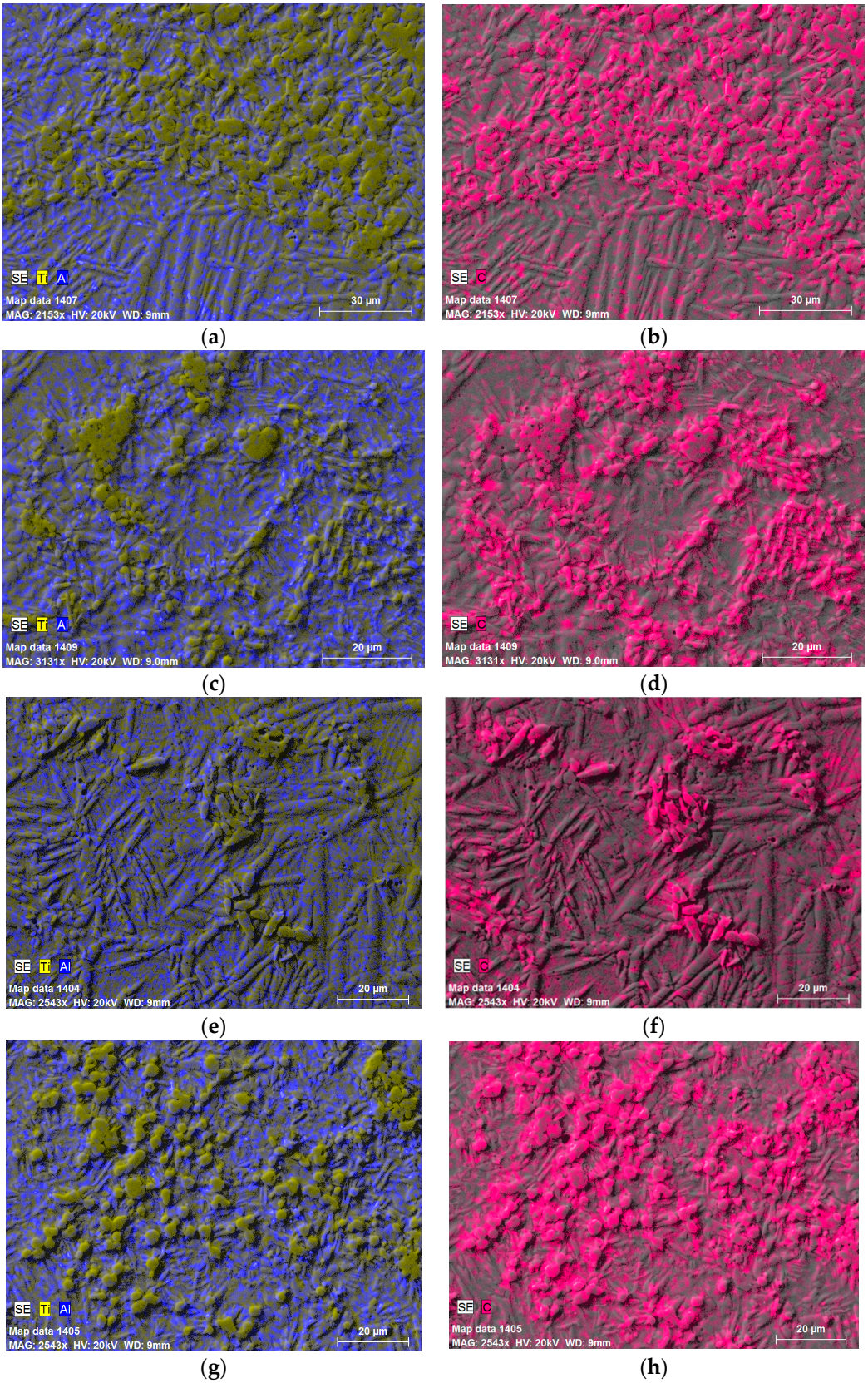

Preprints (www.preprints.org) | NOT PEER-REVIEWED | Posted: 29 November 2023 doi:10.20944/preprints202311.1870.v1

Figure 3. The elemental mapping of the samples: a, b) sample G13, sintered at 950°C; c, d) sample G14, sintered at 960°C; e, f) sample 13, sintered at 985°C; g, h) sample 14, sintered 1020°C.

EDS analysis was performed by analysing separate reinforcing particles: spherical and needle-like fractions (Figure 4), and dispersed unknown elements detected at the grain boundaries – possible titanium carbides, located at the grain boundaries [21]. It was determined that the reinforcing particles mainly consist of titanium, however the peaks of carbon and aluminium are visible, especially when the elongated crystal plates where investigated. These crystal plates could be phases of titanium and aluminium [22].

Some micrographs show contamination with iron, possibly due to the presence of steel electrode (Figure 4a).

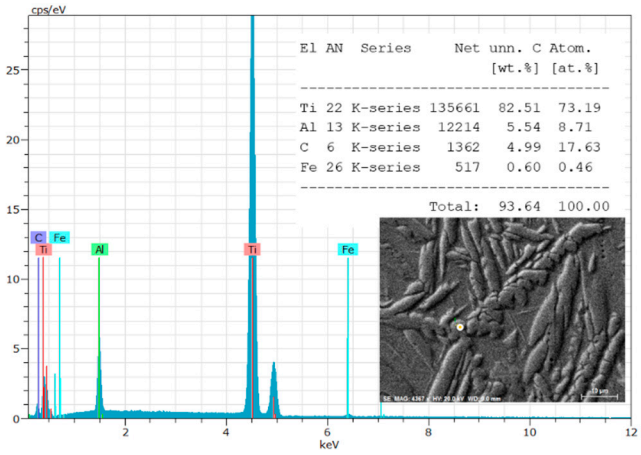

(**a**)

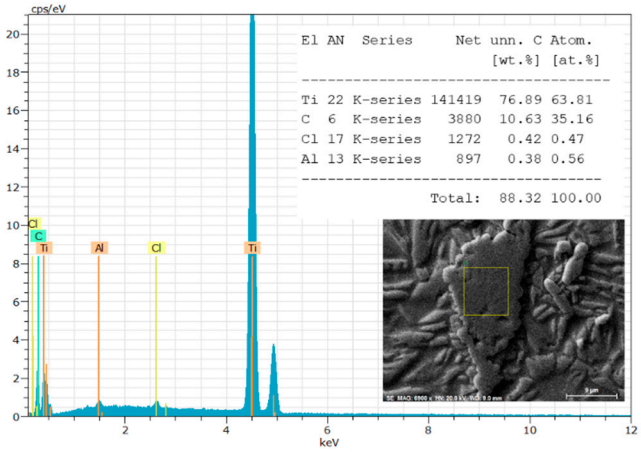

(**b**)

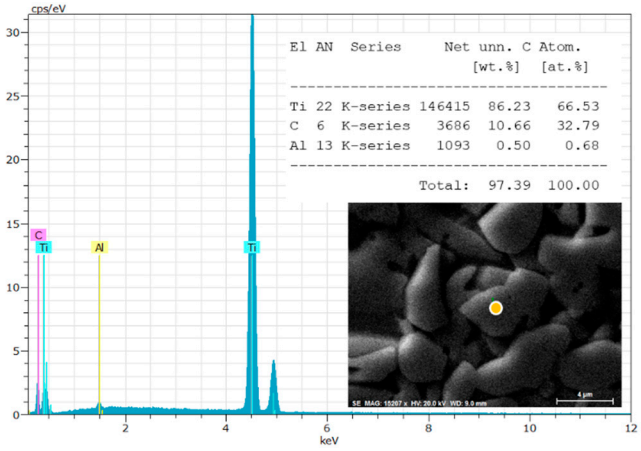

(**c**)

Preprints (www.preprints.org) | NOT PEER-REVIEWED | Posted: 29 November 2023 doi:10.20944/preprints202311.1870.v1

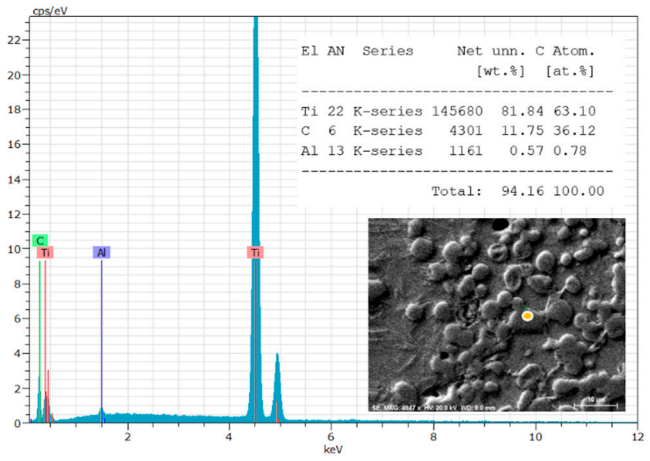

(**d**)

Figure 4. The EDS analysis of the samples: a) sample G13, sintered at 950°C; b) sample G13, sintered 960°C; c) sample 13, sintered at 985°C; c) sample 14, sintered at 1020°C.

Raman spectroscopy was performed on the dark carbide particles, dark big areas, and light grains of the matrix. Raman spectroscopy analysis of the results was made by comparing the values of the intensity of the peaks obtained and the ones found in the literature resources. The review is presented in Table 2.

The results of Raman spectroscopy analysing the Ti-Al-C powder composites are presented in Figure 5.

The results of Raman spectroscopy showed that the dark areas of the Ti-Al-C powder composites revealed the peaks corresponding to the carbon nanostructures like fullerenes C_{60} and C_{70}, graphene or crystalline graphite (Figure 5a,b). The strong peak at about 1580cm^{-1} was detected in all samples, but it is hard to indicate the nature of the carbon nanostructure since some literature resource states that this peak corresponds to the graphene [32,34] and the others – to the crystalline graphite [27,35]. The literature resource [31] proves the existence of graphene which presents peak at about 1555 cm^{-1}. Graphene is believed to be one of the most promising materials that reinforce the metal matrix composites due to its strengthening of the sintered powder materials [24,26,32,34,37].

The areas with small reinforcing particles show different characters of the Raman curves [Figure 5c,d]. The figures present strong peaks at 1555 cm-1 and 1570 cm-1., which could be obtained due to the graphene [28,30,31].

Table 2. The identification of the peaks observed in Raman spectra.

	The position of the peak or the group of the peaks, cm^{-1}	The identification of the peak	The references
	125	Ti_3AlC_2	[23]
1	148-154	Al-C alloy	[24], [25], [26]
	150	Ti_2AlC	[23]
	183, 201	Ti_3AlC_2	[23]
2	208-213	Al(Ti)-C alloy	[24], [25], [26]
3	256-267	Al(Ti)-C alloy	[24], [25], [26]
	262, 268	Ti_2AlC	[23]
4	271-273	C_{60}	[27]
	270	Ti_3AlC_2	[23]
	365	Ti_2AlC	[23]
5	415-431	Al(Ti)-C alloy	[24], [25], [26], [27]
6	488-497	C_{70}	[27], [28]
7	608-613	Al(Ti)-C alloy	[24], [25], [26], [29]
	623	Ti_3AlC_2	[23]

Preprints (www.preprints.org) | NOT PEER-REVIEWED | Posted: 29 November 2023 doi:10.20944/preprints202311.1870.v1

8	632-633	Ti_3AlC_2	[22]
	663	Ti_3AlC_2	[23]
9	771-773	C_{60}	[27], [30]
10	820-840	Al_4C_3	[24]
11	1234-1252	C_{60}	[27], [30]
12	1331	Graphene (D band)	[31]
13	1340	Graphene (D band)	[30]
14	1350	Graphene (D band)	[32], [33], [34]
15	1355-1360	C_{60}	[26]
16	1419-1422	C_{60}	[27]
17	1462-1469	C_{60}	[27], [28]
18	1555	Graphene (G band)	[31]
19	1575-1576	Graphene (G band)	[30], [28]
20	1580-1583	Crystalline graphite	[27], [35]
21	1580-1600	Graphene (G band)	[32], [34]
22	1584-1590	C_{70}	[29], [33]
23	2700-2720	The overtone of the line at 1355 cm^{-1}	[36], [34]
24	2930-2950	Ti-C alloy	[36]
25	2320	Ti-C alloy	[36]
26	2690-2700	Graphene (2D band)	[30], [32], [35]

The peaks observed in the region between 2300cm^{-1} and 3000cm^{-1} refer, probably, to the Ti-C alloy with the exception the peak at about 2713cm^{-1}, which is the overtone of the peak at 1355 (in our case 1346cm^{-1} and 1351cm^{-1}) [36]. One sample showed the peak at about 632 cm^{-1} (Figure 5c) and it could refer to Ti_3AlC_2 [22]. Furthermore, it is determined, that the MAX phase Ti_2AlC, which occurs below 900°C, transforms into MAX phase Ti_3AlC_2 when the temperature increases above 900°C [23]. In our case, sintering temperature is from 950°C to 1020°C, so, the existence of Ti_3AlC_2 could be possible.

Comparing the obtained results with the data found from scientific resources we can conclude that the proposed method of HVED treatment in the kerosene including SPS enables to obtain the metal matrix composites reinforced with the carbon nanostructures that develop the mechanical, electrical, thermal properties, such as heat wear resistance [32,34,37].

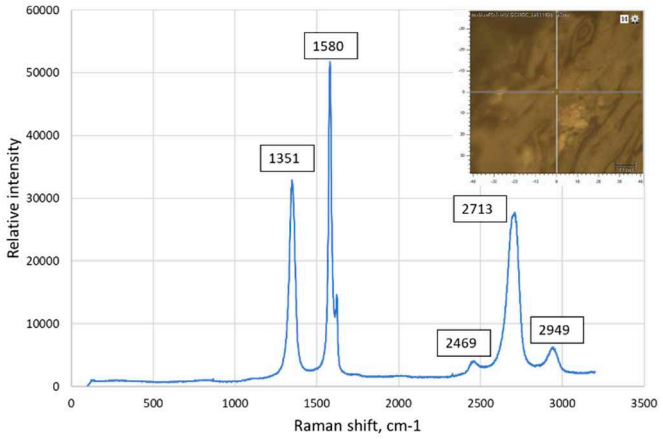

(**a**)

Preprints (www.preprints.org) | NOT PEER-REVIEWED | Posted: 29 November 2023 doi:10.20944/preprints202311.1870.v1

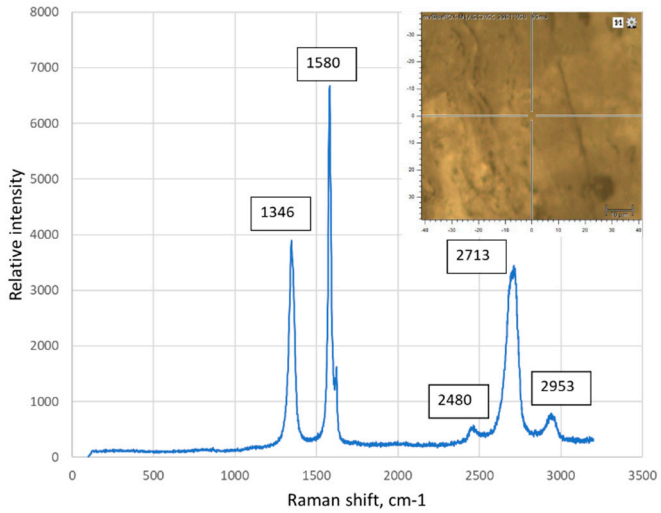

(**b**)

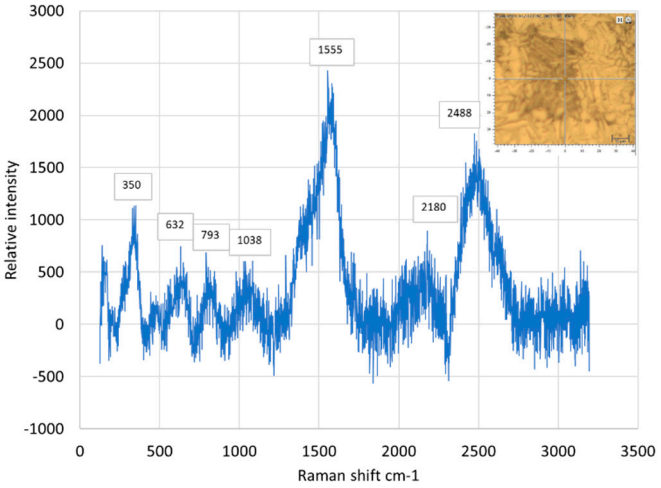

(**c**)

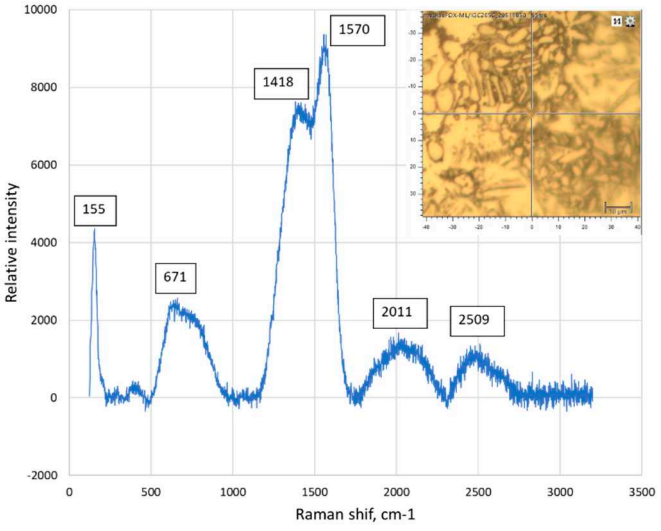

(**d**)

Figure 5. The Raman analysis of the samples with a composition: a) 75% Ti, 15% Al_3Ti, 10% Ti_3AlC_2 sintered at 950°C; b) 70% Ti, 15% Al_3Ti, 15% Ti_3AlC_2 sintered at 950°C; c) 75% Ti, 15% Al_3Ti, 10% Ti_3AlC_2 sintered at 985°C; d) 70% Ti, 15% Al_3Ti, 15% Ti_3AlC_2 sintered at 1020°C.

The detailed phase composition was obtained by X-Ray diffraction (Figure 6). It is worth noting that graphene cannot be detected by X-ray diffraction. Graphene is composed of a single layer

Preprints (www.preprints.org) | NOT PEER-REVIEWED | Posted: 29 November 2023 doi:10.20944/preprints202311.1870.v1

(monolayer) of carbon atoms tightly bound together in a hexagonal lattice [38]. This is an allotropy of carbon. When graphene layers stack on top of each other, graphite is formed. Separated graphene layers in graphite are retained by Van der Waals forces, which can be broken up during exfoliation. Then you get graphene. At least two parallel planes of atoms are required for X-ray diffraction to occur. Therefore, graphene is almost undetectable in the X-ray diffractogram. So, where graphite is identified by XRD, it is graphite. Because the main most intense maximum at 2TH=26.40 degrees shows that the graphene layers are already packed into the graphite lattice.

Considering the carbon nanostructures detected in the Ti-Al-C powder composites, we can conclude that different allotropies of carbon were found in the microstructure – graphene, fullerenes, and graphite.

Two types of the intermetallic phases and one type of carbide were detected existing in the microstructure: $AlTi_3$, Al_3Ti, and TiC, respectively.

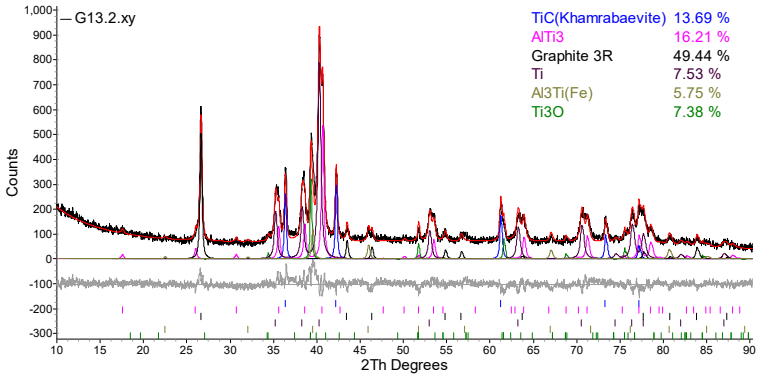

(**a**)

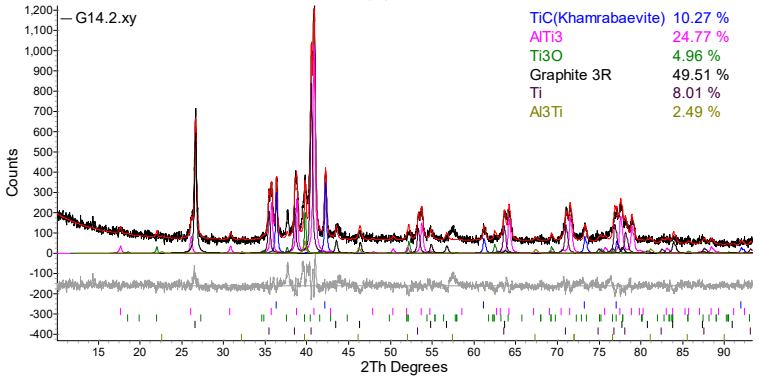

(**b**)

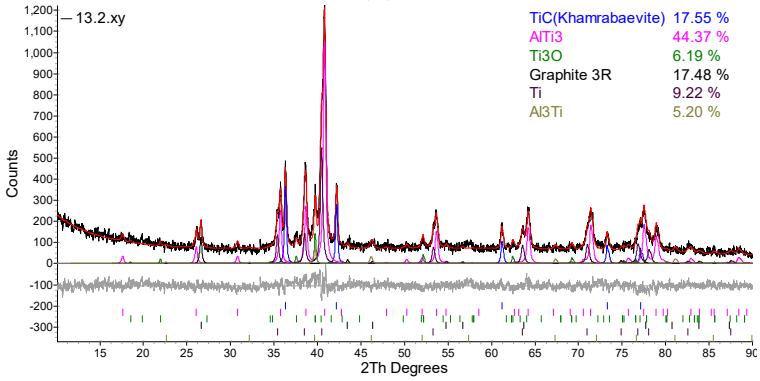

(**c**)

Preprints (www.preprints.org) | NOT PEER-REVIEWED | Posted: 29 November 2023 doi:10.20944/preprints202311.1870.v1

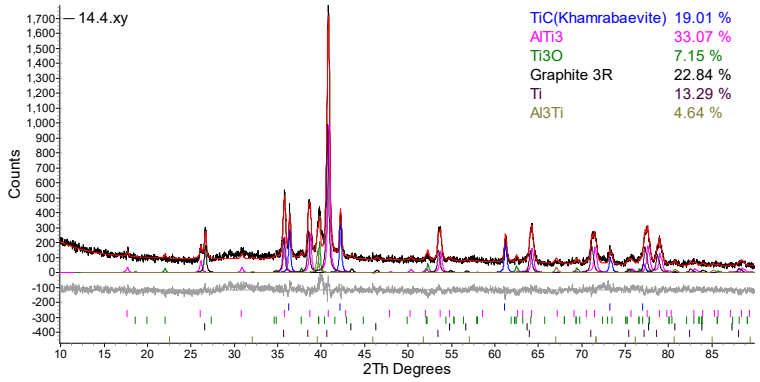

(**d**)

Figure 6. The XRD analysis of the samples: a) sample G13, sintered at 950°C; b) sample G14, sintered at 950°C; c) sample 13, sintered at 985°C; d) sample 14, sintered at 1020°C.

The samples G13 and G14 showed a lot of graphite formed in the composition of the material, then the hardness will decrease, as it did not react with titanium. This means that when processing the powders, the specific energy was higher than necessary and excess graphite appeared. It is necessary to regulate the amount of energy during processing so that there is no excess graphite, and it can all react during processing, and the small amount that remains during sintering. Therefore, the parameters of the technology of HVED+SPS should be improved.

Despite the high content of the graphite, the microhardness measured in the previous work [18] was obtained from 400 to 600 HV. This means that the graphite is equally distributed and does not decrease the mechanical properties of the material.

XRD analysis of the samples showed that they are composed of different amounts of intermetallics like Al_3Ti and $AlTi_3$ (Figure 6). These materials have high melting points, high mechanical strength, oxidation resistance and low densities [39]. The phase composition of the different samples treated under different technological parameters obtained from XRD results are presented in Figure 7. Comparing the contents of Al_3Ti and $AlTi_3$ the $AlTi_3$ is dominant, which is less stable than the Al_3Ti.

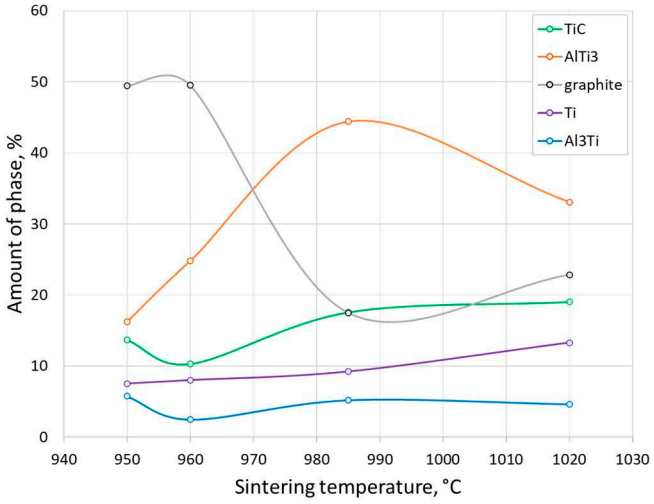

Figure 7. The content of phase composition of Ti-Al-C powder materials depending on the sintering temperature.

5. Conclusions

This research was focused on the dependence of SPS parameters on the final phase composition and microstructure of the Ti-Al-C powder materials. This study investigated the Ti-Al-C composite powder materials produced by SPS consolidation of the powder mixture after the HVED processing

Preprints (www.preprints.org) | NOT PEER-REVIEWED | Posted: 29 November 2023 doi:10.20944/preprints202311.1870.v1

of titanium and aluminium powders in kerosene. An experimental plan was developed which allowed us to establish the relationship between experimental parameters and results.

The SEM analysis showed the microstructure with a big number of reinforcing particles - shape of globular particles and elongated needles distributed randomly in clusters all over the surface as a matrix. Samples have few pores on their surfaces. The lower temperatures gave more pores. The elemental mapping of the Ti-Al-C composite powder materials allowed to determine the distribution of Ti, Al, and C in the microstructure. It was observed that the spherical particles consisted mainly of titanium and carbon since the elongated grains revealed mostly aluminium and less titanium. Here, the line intensity of carbon was obtained to be low. Probably, the phases of TiC and Ti_3AlC_2 were detected, carbide and MAX-phase, respectively.

Raman analysis of the composites revealed the existence of carbon nanostructures in the microstructure. The dominant carbon nanostructure was graphene and fullerenes C_{60} and C_{70}. These nanostructures increase strength and tribological properties of the material. Some detected peaks were not determined and will be investigated in further study.

XRD analysis showed that samples contain such phases like TiC, $AlTi_3$, Al_3Ti and that strengthen material and increase heat resistance of composites. The samples show the formed different amount of graphite depending on the sintering temperature – increasing temperature decreases the excess graphite.

Considering the carbon nanostructures detected in the Ti-Al-C powder composites, we can conclude that different allotropies of carbon were found in the microstructure – graphene, fullerenes, and graphite. The previous investigation showed that the microhardness was sufficient – 400-600 HV, it means that the graphite is distributed equally and does not decrease the mechanical properties of the material. Despite of that, the technological parameters of the HVED+SPS procedure should be improved.

Further investigation of Ti-Al-C composites will be performed according to the tasks of the joint project of Lithuania and Ukraine.

Author Contributions: Conceptualization, R.K.J. and O.S.; methodology, O.S., SEM analysis, R.K.J., XRD analysis R.K.J.; literature review R.K.J., D.M. L.G and I.V; writing—original draft preparation, R.K.J.; writing—review and editing, O.S.; funding acquisition, R.K.J and O.S. All authors have read and agreed to the published version of the manuscript.

Funding: The presented work was performed with partial financial support from the Research Council of Lithuania and the Ministry of Education and Science of Ukraine in the framework of "Application of high-concentrated energy flows for producing nanostructured polyfunctional composite materials" joint project according to the results of joint Ukrainian-Lithuanian R&D projects for the period of 2022 – 2023 contest (Reg. No. P-LUP-22-5).

Acknowledgments: In addition, the authors would like to express their gratitude to the Armed Forces of Ukraine for their bravery which made this work possible even in the dark times of war.

Conflicts of Interest: The authors declare no conflict of interest. The funders had no role in the design of the study; in the collection, analyses, or interpretation of data; in the writing of the manuscript; or in the decision to publish the results.

References

1. Welsch: G.; Boyer, R.; Collings, E. Materials Properties Handbook: Titanium Alloys. ASM international **1993**.
2. Leyens, C.; Peters, M. Titanium and Titanium Alloys: Fundamentals and Applications Weinheim: Chichester: Weinheim: Wiley-VCH; Chichester: John Wiley distributor c2003.
3. Bin, Zh.; Faming, Zh.; Farhad, S.; Caiyun, Sh. Graphene-TiC hybrid reinforced titanium matrix composites with 3D network architecture: Fabrication, microstructure and mechanical properties. *Journal of Alloys and Compounds* **2021**, *859*, 157777. https://doi.org/10.1016/j.jallcom.2020.157777
4. Bakshi, S.R.; Agarwal, A. An analysis of the factors affecting strengthening in carbon nanotube reinforced aluminum composites. *Carbon* **2011**, *49* (2), 533-544. https://doi.org/10.1016/j.carbon.2010.09.054.
5. Singerman, S.; Jackson, J. Superalloys **1996**, eds. R.D. Kissenger, D.J. Deye, D.L. Anton, A.D. Cetel, M.V. Nathal, T.M. Pollock, and D.A. Woodford. Warrendale, PA: TMS. p. 579.

Preprints (www.preprints.org) | NOT PEER-REVIEWED | Posted: 29 November 2023 doi:10.20944/preprints202311.1870.v1

6. Priyaranjan, S.; Pandu, R. V.; Meher, A.; Manas M. M. Recent progress in aluminum metal matrix composites: A review on processing, mechanical and wear properties. *Journal of Manufacturing Processes*, **2020**, *59*, 131-152. https://doi.org/10.1016/j.jmapro.2020.09.010.
7. Bhoi, N.K.; Singh, H.; Pratap, S. Developments in the aluminum metal matrix composites reinforced by micro/nano particles – a review. *JComposMater*, **2020**, *54* (6), 813-833. https://doi.org/10.1177/0021998319865307.
8. Anthony, M.; Schultz, B.F.; Rohatgi, P.K.; Gupta, N. E. A. (Ed.). Metal matrix composites for automotive applications. *John Wiley & Sons* **2014**. https://doi.org/10.1002/9781118535288.
9. Krishan, K. Ch. Carbon Fiber/Carbon Matrix Composites. *Composite Materials* **2019** ISBN : 978-3-030-28982-9.
10. Yuan, Q.; Li, X.; Xu, H.; Song, P.; Lu, J. Microstructure and fracture toughness of in-situ nanocomposite coating by thermal spraying of Ti_3AlC_2/Cu powder. *Ceram. Int.*, **2019**, *45*, 13119-13126.
11. Yu W.B., Zhao H.B., Hu X.S. Anisotropic mechanical and physical properties in textured Ti2AlC reinforced AZ91D magnesium composite. J. Alloy. Compd., 732 (2018), pp. 894-901
12. Yu, W.B.; Wang, X.J.; Zhao, H.B.; Ding, C.; Huang, Z.; Zhai, H.; Guo, Z.; Xiong, S. Microstructure, mechanical properties and fracture mechanism of Ti_2AlC reinforced AZ91D composites fabricated by stir casting. *J. Alloy. Compd.*, **2017**, *702*, 199-208.
13. Liu, A.; Yang, Q.; Ren, X.; Meng, F.; Wu, G. Energy- and cost-efficient NaCl-assisted synthesis of MAX-phase Ti_3AlC_2 at lower temperature. *Ceram. Int.*, **2019**, *46*, 6934-6939.
14. Galvin, T.; Hyatt, N.C.; Rainforth, W.M.; Reaney, I.M; Shepherd, D. Molten salt synthesis of MAX phases in the Ti-Al-C system. *Journal of the European Ceramic Society* **2018**, *38* (14), 4585-4589. https://doi.org/10.1016/j.jeurceramsoc.2018.06.034.
15. Xiaochen, H.;, Yi, F.; Gang, Q.; Hao, Zh.; Jingcheng, Zh.; Xuebin, Zh. Physical, mechanical, and ablation properties of Cu–Ti_3AlC_2 composites with various Ti_3AlC_2 contents. *Materials Science and Technology* **2018**, *34* (6), 757-762. https://doi.org/10.1080/02670836.2017.1407900.
16. Kaczmar, J.W.; Pietrzak, K.; Włosiński, W. The production and application of metal matrix composite materials. *J Mater Process Technol*. **2000**, *106*, 58–67.
17. Magnus, C.; Cooper, D.; Sharp, J.; Rainforth, W.M. Microstructural evolution and wear mechanism of Ti_3AlC_2 – Ti_2AlC dual MAX phase composite consolidated by spark plasma sintering (SPS). *Wear*, **2019**, *438–439*, 203013. https://doi.org/10.1016/j.wear.2019.203013.
18. Kandrotaitė Janutienė, R.; Mažeika D.; Dlouhy J.; Syzonenko O.; Torpakov, A.; Lipian, E.; Baltušnikas, A. Investigation of the microstructure of sintered Ti-Al-C composite powder materials under high-voltage electrical discharge. *Materials* **2023**, *16*, 5894. https://doi.org/10.3390/ma16175894
19. Bruker AXS, TOPAS V4: General Profile and Structure Analysis Software for Powder Diffraction Data. Users Manual, Bruker AXS, Karlsruhe, Germany, 2008.
20. Cheary, R.W.; Coelho, A.A.; Cline, J.P. Fundamental Parameters Line Profile Fitting in Laboratory Diffractometers. *Physics Journal of Research of the National Institute of Standards and Technology* **2004**, *109*(1), pp. 1-25. https://doi.org/10.6028/jres.109.002
21. Shang, C.; Zhang, F.; Wang, J.; Chen, F. Interface configuration effect on mechanical and tribological properties of three-dimension network architectural titanium alloy matrix nanocomposites. *Composites Part A* **2022**, *158*, 106981. https://doi.org/10.1016/j.compositesa/2022.106981.
22. Loupias, L.; Morais, C.; Morisset, S.; Canaff, Ch.; Li, Zh.; Brette, F.; Chartier, P.; Giugnard, N.; Maziere, L.; Mauchamp, V.; Cabioc'h, Th.; Habrioux, A.; Celerier, S. Guideline for synthesis and surface chemistry characterization of 2D Mo/Ti solid solutions based MXene. Application to hydrogen evolution reaction in alkaline media. Preprint.
23. Torres, C.; Quispe, R.; Calderon, N.Z.; Eggert, L.; Hopfeld, M.; Rojas, Ch.; Camargo, M.K.; Bund, A.; Schaaf, P.; Grieseler, R. Development of the phase composition and the properties of Ti2AlC and Ti3AlC2 MAX-phase thin films – A multilayer approach towards high phase purity. *Applied Surface Science* **2021**, *537*, 147864. https://doi.org/10.1016/j.apsusc.2020.147864.
24. Yolshina, L.A.; Muradymov, R.V.; Korsun, I.V.; Yakovlev, G.A.; Smirnov. S.V. Novel aluminum-graphene and aluminum-graphite metallic composite materials: Synthesis and properties. *Journal of Alloys and Compounds* **2016**, *663*, 449-459. http://doi.org/10.1016/j.jallcom.2015.12.084.
25. Choi, H.J.; Shin, J.H.; Bae, D.H. The effect of milling conditions on microstructures and mechanical properties of Al/MWCNT composites. *Composites Part A* **2012**, *43*, 1061-1072. http://doi.org/10.1016/j.compositesa.2012.02.008.
26. Choi, K.; Seo, J.; Bae, D.; Choi, H. Mechanical properties of aluminum-based nanocomposite reinforced with fullerenes. *Transactions of Nonferrous Metals Society of China* **2014**, *24*, s47-s52. http://doi.org/10.1016/S1003-6326(14)63287-8.
27. Luo, Zh.; Loo, B.H.; Yao, J. Uniformly-assembled metal nanoparticles on anodic aluminum oxide (AAO) applied in surface-enhanced Raman spectroscopy. *Mater.Res.Soc.Symp.Proc* **2011**, *1351*. https://doi.org/10.1557/opl.2011.1166.

Preprints (www.preprints.org) | NOT PEER-REVIEWED | Posted: 29 November 2023 doi:10.20944/preprints202311.1870.v1

28. Brett Kimbrell, J.; Crittenden, Ch.M.; Steward, W.J.; Khan, F.A.; Gaquere-Parker, A.C.; Stuart, D.A. Analysis of mixtures of C_{60} and C_{70} by Raman spectroscopy. *Nanoscience Methods* **2014**, *3*, No.1, 40-46. http://doi.org/10.1080/21642311.2014.976776.
29. Chernogorova, O.; Potapova, I.; Drozdova, E.; Sirotinkin, V.; Soldatov, A.V.; Vasiliev, A.; Ekimov, E. Structure and physical properties of nanoclustered graphene synthesized from C_{60} fullerene under high pressure and high temperature. *Appl.Phys.Lett* **2014**, *104*, 043110. http://doi.org/10.1063/1.4863470.
30. Mahmood, S.; ud Din, R.; Khan, M.; Shahzad, M.; Fayas Khan, M.; Akhtar, Sh.; Mateen, A.; Wadood, A. Microstructure, consolidation, electrochemical, and mechanical performance of titanium (Ti) composites reinforced by graphene nanoplatelets (GNPs) via mechanical alloying. *Materials Chemistry and Physics* **2022**, *285*, 126142. http://doi.org/10.1016/j.matchemphys.2022.126142.
31. Bezerra, I.; Freire, P.T.C.; Oliveira, N.C.; Cruz Viana, B. Throwing light on an uncommon preservation of Blattodea from the Crato Formation (Araripe Basin, Cretaceous). *Revista Brasileira de Palentologia* **2018**. https://doi.org/10.4072/rbp.2018.3.05.
32. Wang, H.; Zhang, H.; Cheng, X.; Mu, X.; Chang, Sh.; Feng, K.; Zhang, J. Microstructure evolution and mechanical properties of graphene reinforced Ti-6Al-4V matrix composites: Defective vs high-quality graphene. *Journal of Alloys and Compounds* **2023**, *969*, 172346. http://org.doi/10.1016/j.jallcom.2023.172346.
33. Sizonenko, O.; Prokhorenko, S.; Torpakov, A.; Žak, D.; Lypian, Y.; Wojnarowska-Nowak, R.; Polit, J.; Sheregii, E.M. The metal-matrix composites reinforced by the fullerenes. *AIP Advances* **2018**, *8*, 085317. http://doi.org/10.1063/1.5031195.
34. Wang, H.; Zhang, H.M.; Cheng, X.W.; Chang, S.; Mu, X.N. Effect of ball milling time on microstructure and mechanical properties of graphene nanoplates and TiBw reinforced Ti-6Al-4V alloy composites. *Materials Science and Engineering A* **2022**, *861*, 144240. http://doi.org/10.1016/j.msea.2022.144240.
35. Mallik, A.K.; Das, M.; Ghosh, S.; Chakravarty, D. Spark plasma sintering of Ti-diamond composites. *Ceramics International* **2019**, *45*, 11281-11286. http://doi.org/10.1016/j.ceramint.2019.02.204.
36. Cai, K.J.; Zheng, Y.; Shen, P.; Chen, S.Y. TiC_x-Ti_2C nanocrystals epitaxial graphene-based lamellae by pulsed laser abliation of bulk TiC in vacuum. *CrystEngComm* **2014**, *16*, 5466. https://doi.org/10.1039/c4ce00358f.
37. Chi, F.; Hou, J.; Cui, G.; Zhong, B.; Chen, W. Effects of mixing methods on the interface and microstructure evolution of graphene platelets/Ti-6Al-4V powder composites fabricated by powder metallurgy and extrusion. *Surfaces and Interfaces* **2023**, *36*, 102553. http://doi.org/10.1016/j.surtin.2022.102553.
38. Editorial. All in the graphene family – A recommended nomenclature for two-dimensional carbon materials. *Carbon* **2013**, *65*, 1-6. http://dx.doi.org/10.1016/j.carbon.2013.08.038.
39. Gutierrez, K.; Rodriguez, J.; Array, Y.; Luiggi, N. Topological study of charge density in AlTi, $AlTi_3$ and Al_3Ti intermetallics. *Journal of Computational Methods in Sciences and Engineering* **2012**, *12*, 361-370. https://doi.org/10.3233/JCM-2012-0424.

Disclaimer/Publisher's Note: The statements, opinions and data contained in all publications are solely those of the individual author(s) and contributor(s) and not of MDPI and/or the editor(s). MDPI and/or the editor(s) disclaim responsibility for any injury to people or property resulting from any ideas, methods, instructions or products referred to in the content.